Measuring the Viscoelastic Properties of Human Platelets with the Atomic Force Microscope

Manfred Radmacher, Monika Fritz, Claudia M. Kacher, Jason P. Cleveland, and Paul K. Hansma
Department of Physics, University of California, Santa Barbara, California 93106 USA

ABSTRACT We have measured force curves as a function of the lateral position on top of human platelets with the atomic force microscope. These force curves show the indentation of the cell as the tip loads the sample. By analyzing these force curves we were able to determine the elastic modulus of the platelet with a lateral resolution of ~100 nm. The elastic moduli were in a range of 1–50 kPa measured in the frequency range of 1–50 Hz. Loading forces could be controlled with a resolution of 80 pN and indentations of the platelet could be determined with a resolution of 20 nm.

INTRODUCTION

The cytoskeleton of cells consists of three types of filamentous proteins, actin, microtubules, and intermediate filaments, and a huge variety of associated proteins. These associated proteins control the length of the filaments, their growth or decrease, cross-linking or bundling between filaments, and anchoring of them to the cell membrane or other intracellular compartments. All together these proteins are responsible for the shape of the cell, the movement of the cell, and the generation of force (for a review of the biophysical function see Sackmann, 1994), but they can also have other functions such as the transport of vesicles, which is done by microtubules together with other proteins. Much is known about the viscoelastic properties of in vitro gels of these filamentous proteins (Janmey, 1991), particularly actin; however, little is known about the viscoelastic properties of the cytoskeleton of cells in vivo. One exception is the red blood cell, which has been studied extensively by various methods such as suction with pipettes (Evans, 1989; Discher et al., 1994), flicker spectroscopy (Zeman et al., 1990), and optical tweezers (Svoboda et al., 1992). The cytoskeleton of red blood cells is very different from the cytoskeleton of other cells, because it mainly consists of a two-dimensional sheet, the so-called spectrin network and the cell membrane to which the spectrin network is anchored. Only a few other examples are reported in the literature in which the elastic properties of cells have been measured using a mechanical indenter called a cell poker (Peterson et al., 1982; Zahalak et al., 1990) scanning acoustic microscopy (Hildebrand and Rugar, 1984), (Lüers et al., 1991), fine glass needles (Felder and Elson, 1990), (Adams, 1992), or optical tweezers (Askin and Dziedzic, 1989).

Human platelets are relatively small cells, which play an important role in blood clotting and wound healing. In the bloodstream they are in their resting state, exhibiting a discoid shape. During their activation, for instance at an injury of a blood vessel, a drastic shape change, a reorganization of their cytoskeleton and of receptors, e.g., for fibrinogen, in their membrane occurs. The shape of the fully activated platelet is reminiscent of a fried egg. This activation process could be observed in vitro with the atomic force microscope (AFM) at a resolution of ~50 nm (Fritz et al., 1994a). Although platelets have only a limited metabolism (for instance they are lacking a cell nucleus and thus they cannot synthesize proteins, except the few mitochondrial ones), they show a huge variety in biochemical processes, which make them a very interesting cell in biological and medical studies. The architecture of the cytoskeleton and its rearrangement during activation has been extensively studied by electron microscopy (Hartwig, 1992; Loftus et al., 1984; Albrecht et al., 1989).

The AFM, invented in 1986 (Binnig et al., 1986), has gained some importance for studying biological systems. It is unique because it has proven to be an instrument that can image biological systems at high resolution (in the nanometer range) in their natural aqueous environment. This has been pointed out very early (Drake et al., 1989) and led to very interesting results imaging single molecules like proteins and DNA (Radmacher et al., 1994c; Bezanilla et al., 1994; Yang et al., 1994; Karrasch et al., 1994; for a recent review see Hansma and Hoh, 1994). AFM has been applied to study also living cells in their natural environment (for a review see Henderson, 1994). Recent studies have shown that elastic properties of cells can be detected with the AFM (Hoh and Schoenenberger, 1994). Imaging of elastic properties with the AFM is possible using force modulation (Radmacher et al., 1993; Baselt et al., 1993), which has been applied to platelets (Radmacher et al., 1992) and magnetotactic bacteria (Fritz et al., 1994b). Quantitative analysis of the elastic or other sample properties can be obtained with the AFM by taking force curves, as pointed out earlier (Burnham and Colton, 1989; Weisenhorn et al., 1989, 1992). Recently the binding forces between single mol-

Received for publication 4 May 1995 and in final form 15 September 1995.

Address reprint requests to Dr. Manfred Radmacher, Sektion Physik, Ludwig-Maximilians Universität, Amalienstrasse 54, D-80799 München, Germany. Tel.: 49-89-2180-3545; Fax: 49-89-2189-2050; E-mail: manfred@physics.ucsb.edu.

Dr. Fritz's current address: Lehrstuhl für Biophysik, Technische Universität München, D 85748 Garching, Germany.

0006-3495/96/01/556/12 $2.00

ecules were measured with the AFM (Florin et al., 1994; Lee et al., 1994). The elastic properties of bone and bone marrow (Tao et al., 1992) and gelatin (Radmacher et al., 1995) have been determined with the AFM. The determination of elastic properties can be most easily performed by taking force curves while the tip is raster scanned across the sample (Baselt and Baldeschwieler, 1994; Radmacher et al., 1994b). This mode of operation has been called force mapping.

MATERIALS AND METHODS

Sample preparation

Platelets were prepared from freshly drawn blood of one of us (M. F.) as follows: 100 μl of blood were deposited onto a glass coverslip. After 30 s, the sample was vigorously rinsed with Tyrode buffer (12 mM $NaHCO_3$, 4 mM NaH_2PO_4, 137 mM NaCl, 2.6 mM KCl, 1 mM $MgCl_2$, pH 7.3) to remove all blood cells except the activated platelets that had adhered strongly to the glass. Usually we find only platelets adhered to the glass substrate. The sample was then mounted in the AFM and imaged in Tyrode buffer. No fixation or drying step was involved in the sample preparation.

Instrumentation

AFM was performed with a commercial instrument (Nanoscope III, Digital Instruments, Santa Barbara, CA) for normal imaging. For force mapping the Nanoscope was used together with a second computer for data acquisition of the force curves. The setup has been described previously in detail (Radmacher et al., 1994a). The data were analyzed using IGOR (Wavemetrics, Lake Oswego, OR) and eventually displayed using IMAGE software (Wayne Rasband, National Institutes of Health, Bethesda, MD). Cantilevers were commercially available, soft, silicon nitride cantilevers (Nanoprobe, Digital Instruments, Santa Barbara, CA). The force constants were measured using a previously calibrated cantilever beam made by drawing a glass fiber. The force constant of the cantilevers used in this study were 23 mN/m and 31 mN/m, respectively.

Force mapping

During force mapping, force curves are taken continuously while the tip is scanned laterally over the sample. Force curves were taken typically at 35 Hz, with a 1000-nm scan range; 128 pixels per line were taken at a lateral scan rate of 0.14 Hz, resulting in a total acquisition time of 15 min for the entire data set of 128 × 128 force curves. Lateral scan sizes were usually between 4 and 8 μm resulting in spacing between each force curve of 30 and 60 nm, respectively. The force curves were sampled at 128 pixels, resulting in a vertical resolution of ~8 nm.

Analysis of the measured indentation

A simple model for describing the elastic response of a sample indented by an AFM tip is the Hertz model (Hertz, 1881; Weisenhorn et al., 1992). The most appropriate geometry for the AFM tip in our case is a cylindrical cone with an opening angle α (Radmacher et al., 1995). The Hertz model predicts in the case of an infinitely stiff tip and a soft, flat sample the following relation between indentation and loading force:

$$F = \delta^2 \frac{\pi}{2} \frac{E}{(1-\nu^2)} \tan(\alpha) \tag{1}$$

where F is the loading force, E is the elastic or Young's modulus, ν is the Poisson ratio, α is the opening angle of the cone, and δ is the indentation depth. The model also predicts the contact area as a function of the loading force:

$$r = \sqrt{F \frac{2}{\pi * \tan(\alpha)} \frac{(1-\nu^2)}{E}} \tag{2}$$

where r is the radius of the contact area.

In a force curve on a sample that is very stiff compared with the spring constant of the cantilever the deflection d will be equal to the sample height z:

$$z = d \tag{3}$$

On a soft sample the z movement of the sample will cause a deflection of the cantilever and possibly an indentation δ of the sample, so Eq. 3 has to be modified accordingly:

$$z = d + \delta \tag{4}$$

In both cases the loading force F will be given by the deflection of the cantilever multiplied by the force constant k of the cantilever:

$$F = k \times d \tag{5}$$

We can use Eq. 5 for reformulating Eq. 1 using the measurable quantity d, the cantilever deflection:

$$k \times d = \delta^2 \frac{\pi}{2} \frac{E}{(1-\nu^2)} \tan(\alpha) \tag{6}$$

Equation 6 can be rearranged so that we get an expression for the indentation, which can be used in Eq. 4 for replacing δ.

$$\delta = \sqrt{\frac{k}{(\pi/2)[E/(1-\nu^2)]\tan(\alpha)}} \sqrt{d} \tag{7}$$

$$z = d + \sqrt{\frac{k}{(\pi/2)[E/(1-\nu^2)]\tan(\alpha)}} \sqrt{d} \tag{8}$$

This is finally the mathematical function describing the force curve as measured on a soft sample. To obtain values for the elastic properties we have first to determine independently the force constant k of the cantilever and its opening angle α. Then we can use Eq. 8 for fitting the measured data and getting a value for the elastic modulus E. Because in the measured data the zeros of the deflection and of the sample height are not well defined we have to rewrite Eq. 8 more generally:

$$z - z_0 = d - d_0 + \sqrt{\frac{k}{(\pi/2)[E/(1-\nu^2)]\tan(\alpha)}} \sqrt{d - d_0} \tag{9}$$

where z_0 and d_0 are the offsets of the sample height and the deflection, respectively. The offset of the deflection d_0 can be easily determined by calculating the mean deflection at the very beginning of the force curves (typically the first 100 nm), where the cantilever is off the surface. Determining the offset of the sample height is easy with force curves on stiff substrates but is more difficult with the force curves on the soft samples because they do not show a sharp kink in the deflection.

Unfortunately, Eq. 9 is of such a form that an analytical least squares fit to determine the two fit-parameters E and z_0 cannot be performed. A possible alternative would be doing a Monte Carlo fit with reasonable starting values. It turned out that the signal-to-noise ratio of the measured data is very good, so that the two parameters can be obtained much easier. We need to take two height values with their corresponding deflection values and enter them in Eq. 9. These two data points set up two equations that can be inverted to obtain values for the elastic modulus E and the offset

z_0 of the height. The fitted data shown below are determined by this method and show the quality of this very simple fit method.

RESULTS

Fig. 1 shows an AFM image taken of a partially activated platelet. The platelet is adsorbed on a glass cover slide. The image shows several distinct regions of the cell: the high

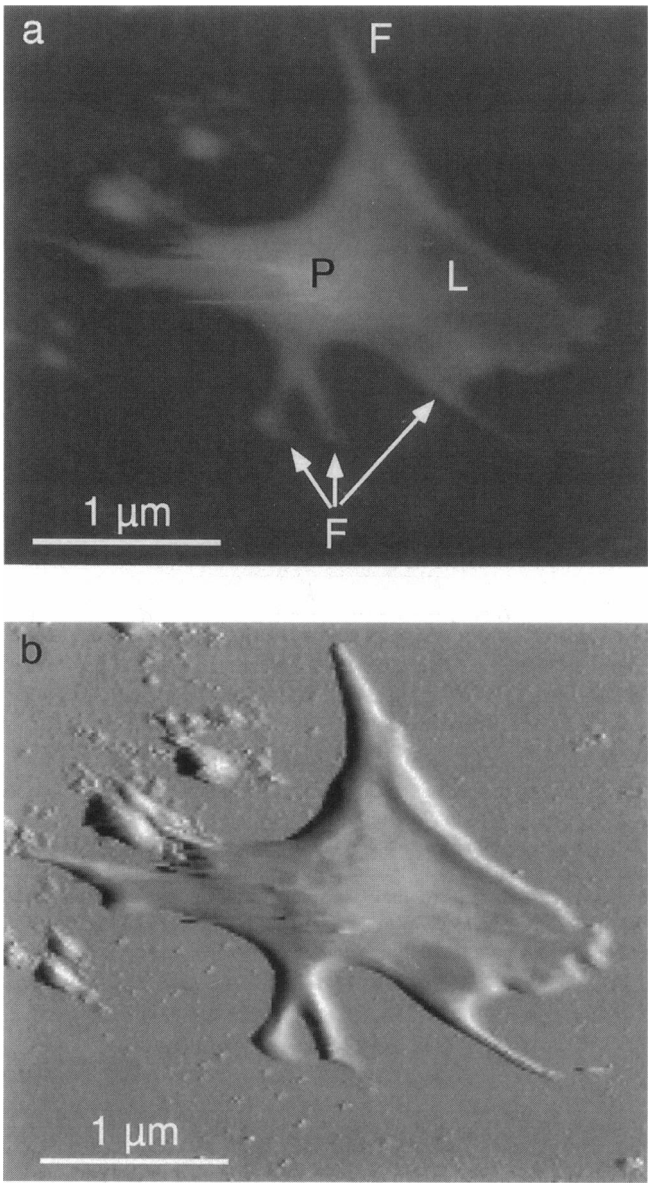

FIGURE 1 Conventional AFM image of a human platelet activated and adhered to a glass coverslip. The image is taken in constant force mode at a loading force of ~1.1 nN. (*a*) Height signal, corresponding to the output of the AFM feedback, which is trying to maintain a constant loading force. (*b*) Error signal. As the feedback always reacts with a little time delay, there will be small variations in the loading force visible while monitoring the cantilever deflection (Putman et al., 1992). This is actually a convenient way of splitting the available information in one image with the overall topography (*a*) and a second image with the small corrugations on the sample (*b*). In *a*, the pseudonucleus (P), several filopodia (F), and a lamellipodium (L) are labeled.

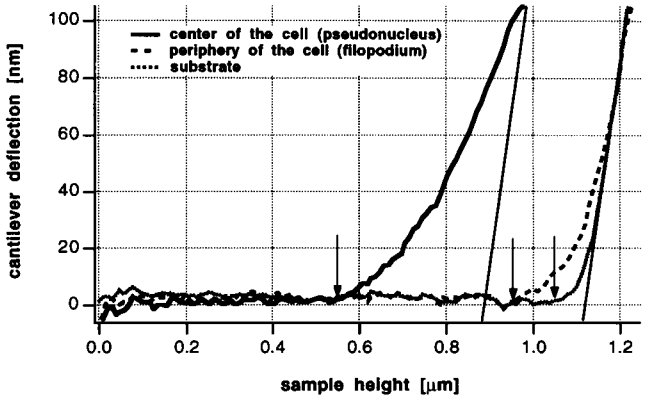

FIGURE 2 Figure 2 shows several force curves taken on different spots on a platelet and on the glass substrate, respectively. The arrows denote the point of contact and demonstrate how the topography can be determined by analyzing force curves. The force curve taken on the substrate shows basically two linear regions: (1) a horizontal part at the left, where the tip is not touching the sample and thus the deflection is constant and (2) a sloped part at the right, where the tip touches the sample and thus the cantilever deflection is proportional to the sample height. The deflection of the cantilever increases less while the sample height is changed due to indentation of the sample. This is visible as a smaller and changing slope of the contact part of the curves taken on the pseudonucleus and the filopodium. As the filopodium is very thin (~100 nm), eventually it has been fully compressed and the slope of the force curve becomes identical with the slope on the stiff substrate. On the much higher pseudonucleus this is not observed.

pseudonucleus (P), also called the granulomere, several filopodia (F) spreading out in different directions, and a large and very flat lamellipodium (L). Fig. 2 shows force curves taken on different regions of another platelet: on the pseudonucleus, on a filopodium, and on the substrate. In a force curve the sample height is changed periodically while the deflection of the cantilever is monitored. On a stiff sample the force curve basically shows two regions: (1) the off-surface part, where the tip is not touching the sample and thus the deflection stays constant (to the left in the traces of Fig. 2) and (2) the in-contact part where the cantilever is defleted proportional to the sample height, resulting in a sloped part of the force curve (to the right in the traces of Fig. 2). In the case of soft samples, the measurable deflection can be smaller than the movement of the sample due to indentation of the sample (see the force curve taken on the pseudonucleus in Fig. 2). This indentation can be elastic in nature, as discussed below. In force curves the deflection of the cantilever is proportional to the loading force and the deviation of the deflection from the slope obtained on a stiff substrate is the sample indentation. Thus indentation versus loading force curves can be calculated from the measured force curves. The elastic indentation of the sample results in a nonlinear force curve that can be modeled using a simple tip and sample geometry as will be pointed out below. In a previous work we explained this procedure in great detail and showed that the tip is best approximated by a cone of a given opening angle at indentations larger than 10 nm (Radmacher et al., 1995). With

this model the elastic modulus of the sample can be obtained. The force curve taken on the filopodium shows a behavior in between the curves measured on the substrate and the pseudonucleus, respectively. At low loading forces (corresponding to small deflections of the cantilever) the nonlinear force curve of a soft sample is visible, as on the pseudonucleus. At higher loading forces, corresponding to deflections larger than 40 nm, the slope is identical to the slope on the substrate, showing that the sample is now as stiff as the substrate. This suggests that the cell has been entirely compressed so that the tip feels the stiffness of the underlying substrate. We will come back to the consequences of this behavior while discussing Figs. 10 and 11.

Hydrodynamic drag

For technical reasons (total time for acquiring one set of force curves) force curves were taken at rates between 25 and 50 Hz for force mapping. At these high scan rates the soft cantilevers used bend drastically due to hydrodynamic drag exerted by the liquid. This effect can be seen as a separation of the off-surface parts of the force curves taken while approaching and retracting from the surface (Hoh and Engel, 1993). Fig. 3 shows a set of force curves taken on the substrate at different scan rates between 1 and 20 Hz. The separation becomes larger when the scan rate increases. To support the hypothesis that the observed effect is caused by hydrodynamic drag of the liquid, we plot the separation between the approach and the retract traces as a function of the scan velocity with which the sample is moved up and down during the force curve. As the separation in the two traces is caused by a bending of the cantilever it is related to a force that the liquid exerts on the cantilever. In the case of a Newtonian liquid the friction force will be proportional to the velocity. Fig. 4 shows the observed separation between approach and retract as a function of the scan velocity of the corresponding force curve. The relation is obviously linear

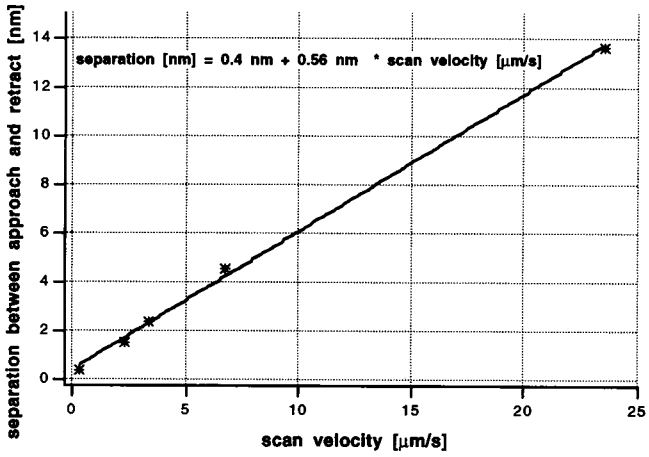

FIGURE 4 The separation between approach and retract traces in force curves as measured in the off surface region is plotted versus the scan velocity used for taking the corresponding force curve. The relationship between the two is clearly linear, supporting the hypothesis that the observed effect is caused by hydrodynamic friction. Hydrodynamic friction will be proportional to the velocity. We conclude that hydrodynamic drag will just exert a constant external force on the cantilever with changing sign, when the direction of the movement of the sample is reversed. An easy procedure to account for this external loading force is averaging the approach and retract traces and using this averaged trace in the following analysis.

showing the appropriateness of our model. Therefore we conclude that the hydrodynamic drag adds a constant external force to the loading force of the cantilever. The sign of this external force will change when the direction of movement is reversed between approach and retract. One way of dealing with this force offset in the analysis is averaging the force curves obtained during approach and retract. (A thorough analysis would show that before averaging the force curves they have to be shifted against each other by the amount of the separation of the cantilever. As this separation is only ~10 nm and the range of sample movement of the force is ~1 μm we neglect this second order correction here).

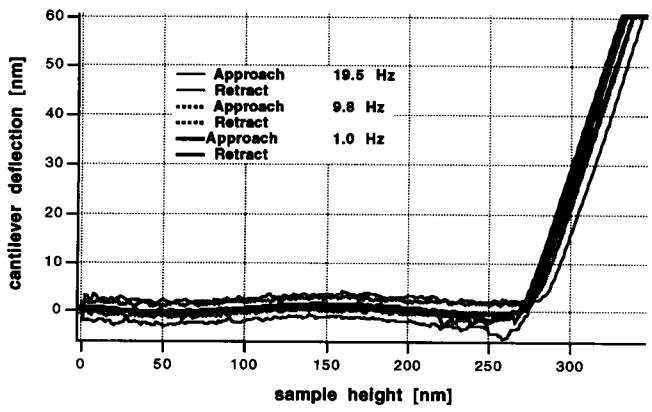

FIGURE 3 Three force curves on the substrate taken at different scan rates. Due to hydrodynamic drag of the water the cantilever is bent in a different direction while the sample is approaching the tip or is being retracted from the tip. This bending is visible as an increasing gap between the approach and retract traces when the scan rate is increased.

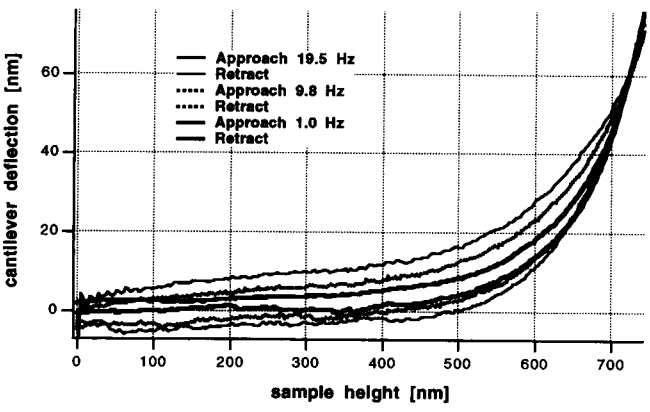

FIGURE 5 Force curves taken on the same spot of a human platelet with different scan rates. Here, we also see an increasing separation of the approach and retract traces as the scan rate is increased. However, as these curves are highly nonlinear because of elastic indentation the interpretation as hydrodynamic drag is not so obvious as it was with the force curves taken on the substrate (Fig. 3).

Fig. 5 shows a set of force curves taken on the pseudonucleus of a platelet at different scan rates. As these force curves are now highly curved due to elastic indentation the effect of the hydrodynamic drag is not as clearly understandable as in Fig. 3. However, after averaging the approach and retract traces of each force curve, all of these averaged force curves lie on top of each other (Fig. 6), demonstrating that the procedure developed above can be applied on these force curves. For comparison the averaged force curves are plotted together with the force curve taken at 20 Hz, exhibiting the largest separation.

Viscous response of the platelet

This apparently technical result is actually very interesting. Until now we were considering only viscous effects of the surrounding liquid, which was fully justified in the case of the glass substrate. In the case of the platelet, the cell itself could show some viscous effect, which would result in a dependence of the force curve on the scan velocity. As our data show no dependency on the scan rate in the averaged curves we conclude that in our measurements the cells react mainly elastically; we cannot detect any viscous behavior of the cell for force curve frequencies up to 20 Hz. However, a refined method of measuring that is also sensitive to viscous effects might reveal interesting features not observable in our data. This result is actually not surprising considering measurements done on actin gels. In the frequency range used here the loss modulus, which is a measure of the viscous response, tends to be two orders of magnitude smaller than the storage modulus, a measure of the elastic response (Janmey et al., 1994).

Elastic response of the platelets

Fig. 7 shows all the force curves taken while scanning along one line over a platelet. The force curves are stacked one behind the other forming a force relief. The vertical axis in this graph corresponds to the cantilever deflection, the horizontal axis corresponds to the sample height, and the axis pointing to the rear corresponds to the lateral position at which the force curve has been taken. In this relief several regions can be distinguished. The force curves shown in the front of this graph were taken on the substrate and show two linear regions, one where the deflection is constant when the tip does not touch the sample and another where the deflection is proportional to the sample height when the tip is touching the sample. Behind these curves we see curves where the tip is touching the sample earlier. These curves are taken on the cell, which is naturally higher than the substrate. The first curves taken on a filopodium show, at higher loading forces, a slope similar to the slope on the substrate, as has been pointed out already in Fig. 2. Finally, this figure shows curves taken on the cell body, which appears very soft. To guide the eye we painted this relief with shades of gray corresponding to lines of constant deflection, meaning constant loading forces. Following the lines that divide gray regions we get a trace of the topography at constant force.

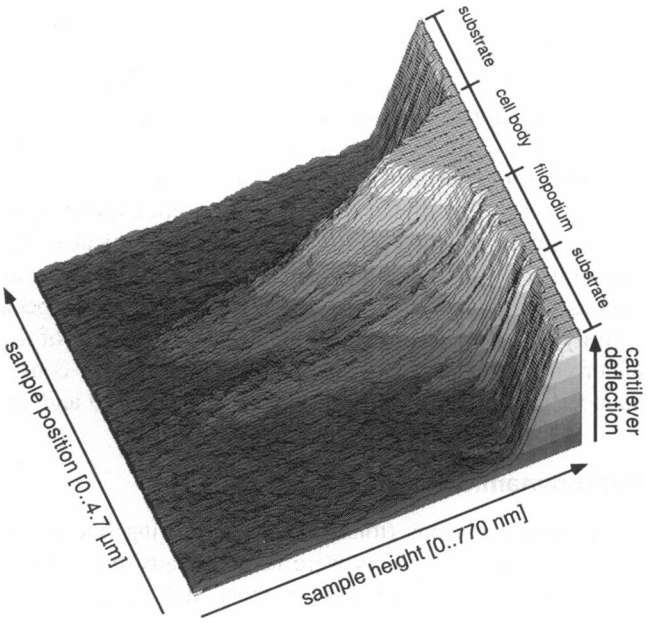

FIGURE 7 All of the force curves taken while scanning along one line over a platelet. In this relief several regions can be distinguished nicely; to the front the force curves were taken on the stiff substrate, then force curves were taken on a filopodium, and finally force curves were taken on the highest part of the cell, the cell body. The lines that divide gray shades correspond to constant force traces. Following one of the gray regions we will follow all the force curves along one given deflection value, which corresponds to a given loading force. Thus this line is a topographic trace at constant loading force.

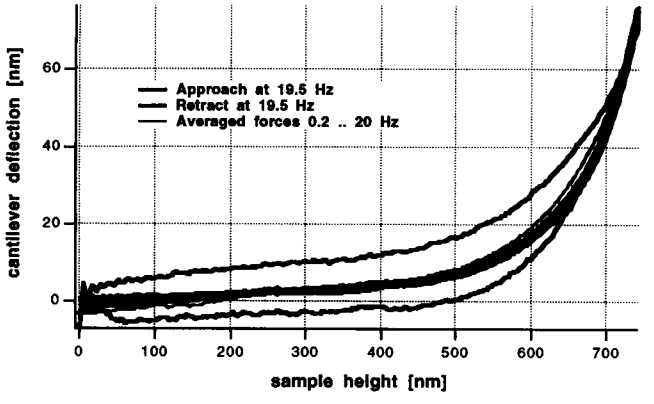

FIGURE 6 Averaged force curves, obtained by averaging the data presented in Fig. 5 together with the approach and retract traces recorded at the highest scan rate. All the averaged traces line up on top of each other showing that no visible difference can be found between force curves taken between 0.2 and 20 Hz. This shows that the response of the platelet to the loading of the AFM tip as seen in a force curve is mainly elastic.

Fig. 8 shows a collection of these topographic traces at different locations on the cell. The traces in one graph correspond to the topography of the same scan line as measured with different loading forces. It has to be pointed out here that the temporal order of data acquisition is

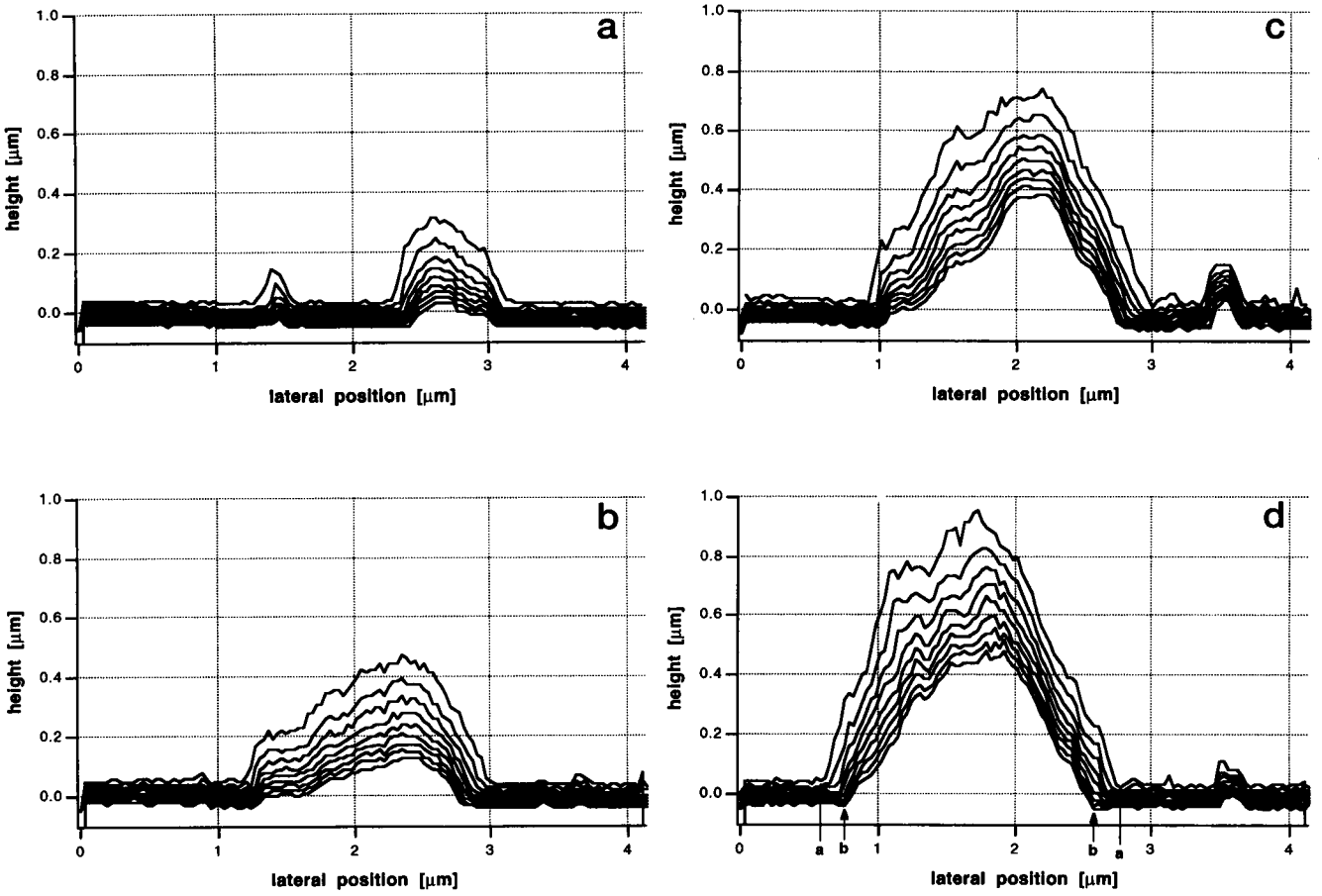

FIGURE 8 As described in Fig. 7, topographic traces at constant force can be calculated from force curves. This has been done here for several scan lines (*a–d*) and for several loading forces in each line. The loading forces are ~0.4 nN for the top-most trace and increase by 0.4 nN for each trace, resulting in a final loading force of 3.6 nN for the bottom-most trace. These sets of traces show how different parts of the cell are compressed when the loading force is increased. It can even happen that the cell is compressed so far that the height is not distinguishable any more from the substrate (see for instance the *arrows* in *d*, which denote the width of the cell at lowest (*a*) and at highest (*b*) forces). This will have the consequence that the cell appears smaller in an image.

different from what this graph might suggest. We recorded a force curve on one spot on the sample and then moved to the next spot on the sample to take the next force curve. Therefore the height values of all the traces at the same position are taken more or less simultaneously and the height values at different positions, even of the same plot line in this figure, are taken with a time delay. This shows that we could stably probe the mechanical properties of the platelet without disturbing or destroying the cell. The difference in loading force between two adjacent traces is 0.4 nN. The loading forces range from ~0.4 nN to a maximal force of 3.6 nN. There is a substantial compression of the cell visible of roughly one-half of the initial height. These traces show that there are significant differences in the elastic properties of the cell depending on the position. This will be discussed further below. Another effect that is visible in these traces is that the apparent width of the cell can decrease at higher loading forces. See for instance the arrows in Fig. 8 *d*. The width of the cell has decreased from 2.2 μm at the lowest loading force (0.4 nN) to 1.8 μm at the highest loading force (3.6 nN). This shows that some parts of the cell have been compressed so much that the remaining height difference to the substrate is not visible any more with our instrument. In our case the resolution in height is worse than in usual AFM and depends on the number of pixels used for sampling the force curves. The theoretical resolution limit with our imaging parameters is ~10 nm; a reasonable value is probably 20 nm. Again, the temporal order of data acquisition is important here. The cell is compressed very much during a force curve and then the tip is moved to the next spot and the cell basically shows the same behavior. This means the cell relaxed and recovered fully after a force curve, showing that the observed compression is reversible and nondestructive to the cell.

The effect of the loading force on the image obtainable in AFM is more obvious in Fig. 9. As demonstrated for line traces in Fig. 8, it is possible to reconstruct constant force images out of the complete data set of force curves as a function of lateral position. Each force curve is analyzed such that the height value at a given loading force, corre-

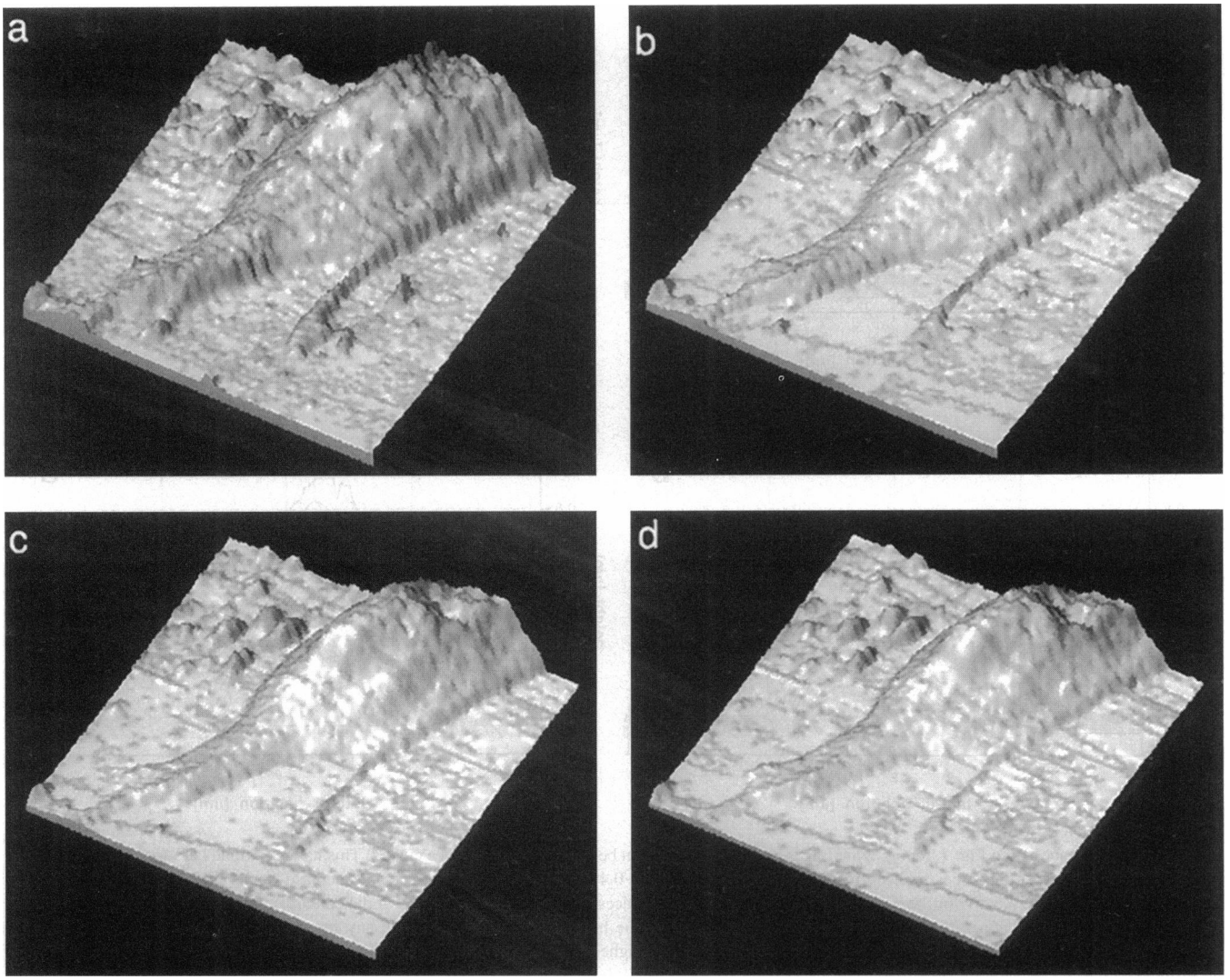

FIGURE 9 Constant force topograph from all force curves recorded while scanning laterally over a human platelet. The loading force increases from ~0.4 nN in *a* to 1.2 nN (*b*) to 2 nN (*c*) to, finally, 2.8 nN *d*. The imaged area is 4.3 μm by 4.3 μm. Note that the cell is compressed and that the small corrugations disappear when the loading force is increased.

sponding to a given deflection value, is calculated. These height values as a function of lateral position resemble the surface relief of the cell. This relief can be displayed in several ways, for instance using a surface rendering algorithm, which created the images in Fig. 9. Fig. 9 *a* is the constant force relief at very small loading forces (~0.4 nN). The force is increasing through Fig. 9 *d* at steps of 0.8 nN (Fig. 9 *b*, 1.2 nN; 9 *c*, 2.0 nN; 9 *d*, 2.8 nN). The cell becomes flatter while the loading force is increased and a lot of the surface corrugations visible in Fig. 9 *a* are smoothed out or disappear totally. These images are similar but not identical to constant force images obtained usually in AFM. In a standard AFM image the tip scans fastest laterally over the sample while a feedback tries to keep the deflection, which is proportional to the loading force, constant. In this imaging mode lateral forces are always present, which might contribute to the contrast or might push around the sample or could even remove the cell from the substrate. Practically, we were not able to obtain an image at forces less than 1 nN in normal contact mode. Therefore the image of Fig. 9 *a* could not be obtained with a conventional AFM. On the other hand, imaging forces as high as in Fig. 9 *d* usually would destroy or remove the cell after a few scan lines. So, for imaging of cells with a conventional AFM there is only a small window of forces accessible. The lack of lateral forces is quite understandable in force mapping mode, as the tip is moved up and down quickly while the sample is scanned laterally very slowly. So, between two adjacent positions, the tip always becomes free of the sample. It is, however, perhaps surprising that the cell can withstand the high loading forces during each force curve, which leads to a considerable compression of the cell. Taking into account the huge number of force curves taken on each cell (several thousands) this becomes even more surprising.

Quantifying the elastic response of the platelet

Fig. 10 shows how the apparent elastic response of the platelet to the loading of the tip, as shown in the topographic traces of Fig. 8, can be theoretically modeled and quantified. The elastic response of a soft sample indented by an AFM tip can be simply described with the Hertz model with an appropriate geometry for the sample and the tip. The simplest geometry uses a flat, soft, and isotropic sample and a conical tip. This model has been demonstrated to be appropriate for AFM at indentations larger than 10 nm (Radmacher et al., 1995). The assumption of an isotropic sample might not be justified in the case of platelets, but in this first study we want to use it. Future work might take into account the local differences and the anisotropic arrangement of the constituents of the cytoskeleton. The force curves can be analyzed in the following way. On a stiff spot of the sample, the deflection of the cantilever will be proportional to the sample height. On a soft spot the deflection will be smaller due to elastic indentation of the sample. This indentation can be plotted versus the loading force, which is the cantilever deflection multiplied by the force constant of the cantilever. This has been plotted in Fig. 10 for the three force curves previously shown in Fig. 2. These indentation versus loading force curves can then be modeled by the Hertz model, as shown by the dotted traces in Fig. 10. The model resembles nicely the measured traces. As the Hertz model is assuming a homogeneous and infinitely large sample it can be appropriate only as long as the indentation is smaller than the thickness of the sample. This explains the discrepancy of the model and experimental data in the case of Fig. 10 *a*, the force curve taken on the filopodium, at high loading forces. There is very good agreement even up to high indentations at the thicker parts of the cell (Fig. 10 *b*, taken on top of the pseudonucleus).

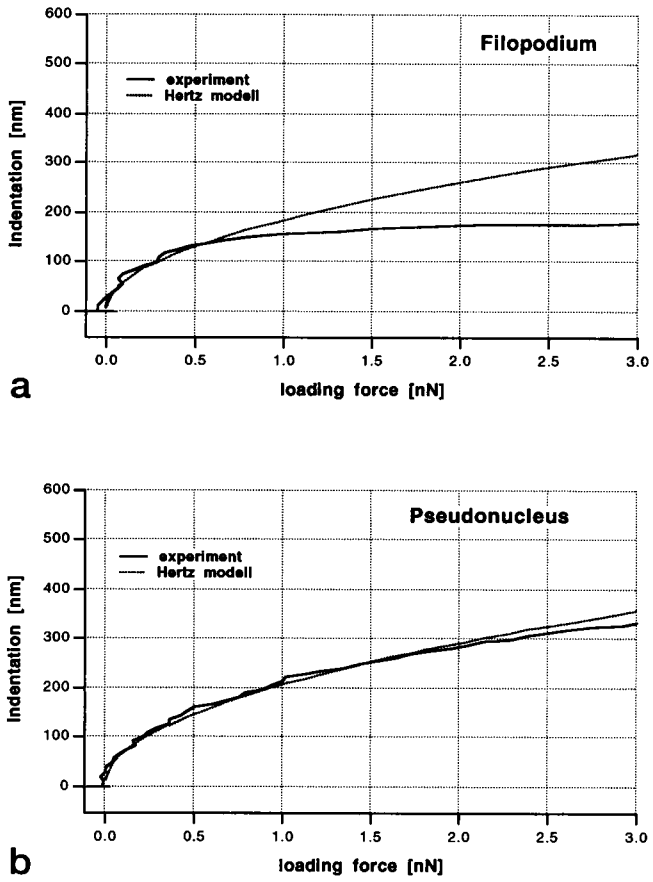

FIGURE 10 How the elastic response of the cell can be modeled. (*a* and *b*) Indentation versus loading force relation of the force curves shown in Fig. 2. (*a*) Indentation measured on the filopodium. (*b*) Indentation measured on the pseudonucleus. The measured indentation versus loading force can be nicely modeled with the Hertz model for small loading forces in the case of the filopodium and over the entire data range on top of the pseudonucleus. The poor fit on the filopodium at high loading force can be understood as follows: the filopodium is a relatively thin structure, which can eventually be fully compressed. This effect has been pointed out in Fig. 2 already. Then the tip feels the underlying stiff substrate and the indentation will not increase very much any more with loading force. This shows that care has to be taken to choose a reasonable range of loading forces to analyze the force curves. This will be discussed in detail in the next figure. (Parameters for the fit are as follows: conical tip with an opening angle of 30°; Poisson ratio, 0.5; force constant of the cantilever, 0.031 N/m; elastic modulus of 9.3 kPa (*a*) and 10.9 kPa (*b*)).

The traces in Fig. 10 show the danger of a possible artifact in analyzing and modeling force curves as described. If the range of the force curve used for analysis is picked such that the sample is substantially compressed already and the tip feels the underlying substrate, the values of the elastic modulus will not be right. This obviously happens if the indentation versus loading force shown in Fig. 10 *b* is analyzed at loading forces corresponding to cantilever deflection between 20 and 40 nm. The hope is that at smaller deflections, such as ~10 nm, the tip does not feel the underlying substrate and good values for the elastic modulus of the sample can be obtained. Experimentally, this artifact can be checked by analyzing different parts of the force curves and comparing the obtained values of the elastic modulus to each other. This is shown in Fig. 11, which shows traces of the topography (solid line) and the calculated elastic moduli, obtained from analyzing different parts of the force curve. The value of the elastic modulus obtained by analyzing the portion of the force curves with the cantilever deflection between 20 and 40 nm resembles the topography and shows clearly the artifact discused above. Analyzing portions of the force curve at smaller indentations (10–20 nm, 5–15 nm, 5–10 nm) show that here the values become identical to each other and do not resemble the topography any more (Fig. 11 *a*). Fig. 11 *b* shows the same data with a different axis for the elastic modulus, so that the values obtained by analyzing the portions of the force curve at low loading forces can be compared easily. Fig. 11 *c* shows the topography and the elastic modulus of another scan line. In this line the elastic modulus and the topography seem to be independent of each other, demonstrating the value of our data analysis.

Fig. 12 shows a map of the topography and the elastic modulus reconstructed from force curves. To fit the range and the variability of values for the elastic modulus in this graph we encoded the logarithm of the elastic modulus in

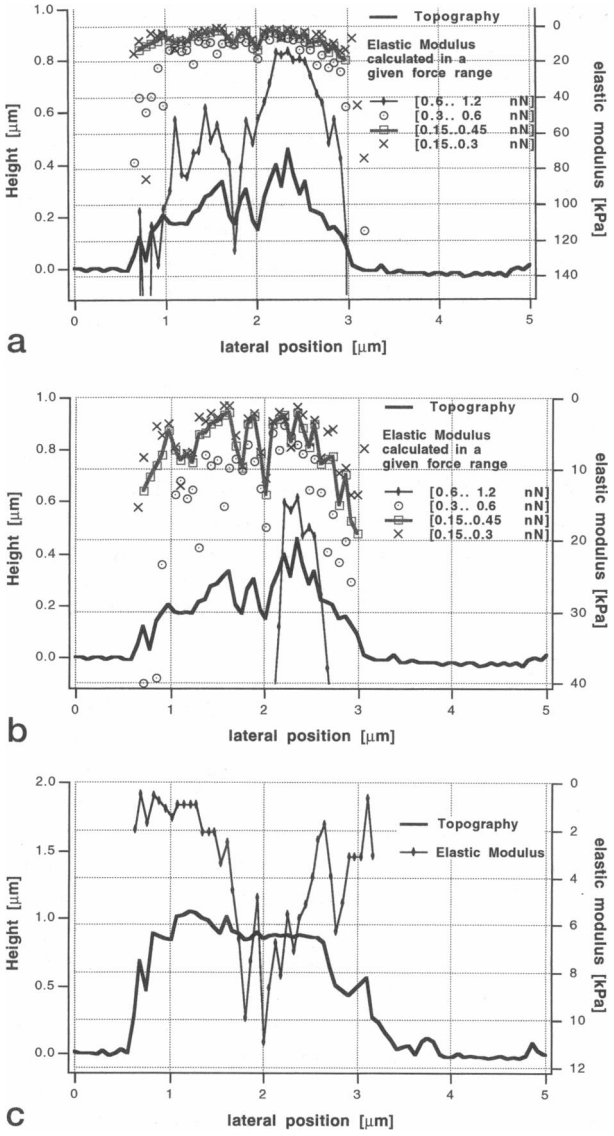

FIGURE 11 Topography along one line together with the calculated elastic modulus along the same line. Different parts of the indentation versus loading force curves were used for determining the elastic modulus, as pointed out in Figure 10. Using the range of loading forces between 0.6 and 1.2 nN, the calculated elastic modulus basically only resembles the topography. This is the artifact, pointed out above, that is generated if the tip feels the stiffness of the underlying substrate. This artifact is prominent on thin portions of the cell, as shown here. Using portions of the indentation versus loading force corresponding to smaller loading forces (0.15–0.3 nN, 0.15–0.45 nN, 0.3 nN-0.45 nN) results in elastic moduli that are close to each other and are relatively independent of the topography. (*b*) The same data with a different range on the axis for the elastic modulus to emphasize that the obtained values of the elastic moduli are independent of the range of loading force used as long as the maximal loading force is smaller than 0.45 nN. We will use from now on a range of 0.15 to 0.45 nN for analyzing the force curves and obtaining values for the elastic modulus. (*c*) Topography and the elastic modulus along another scan line, where one clearly sees the independence of topography and elastic properties.

gray codes. Black corresponds to 100 kPa, white to 1 kPa, and a medium gray to 10 kPa. There is a strong correlation with the height of the cell (Fig. 12 *a*) and the elastic modulus (Fig. 12 *b*). However, there are certain deviations from this trivial connection that are very interesting and will be discussed below.

DISCUSSION

We could demonstrate here that the elastic properties of cells can be measured with the AFM. Several surprising results have been obtained. (1) The cell can withstand relative large loading forces (up to 3 nN) acting on a very small area of the order of 100 nm diameter and less. With Eq. 2 we can estimate the radius of the contact area and get values between 20 and 75 nm for a loading force of 1 nN, a Poisson ratio of 0.5, an opening angle of 30°, and an elastic modulus of 1 and 10 kPa, respectively. This corresponds to an estimated mean pressure exerted by the tip onto the sample of 0.6 and 8 kPa, respectively. It is very surprising that the cell can withstand such high local pressures. But, as we could record several thousands of force curves on the same cell without any noticeable change in the response of the cell to the indenting tip, the cell definitely can withstand these forces and pressures. This raises the questions of how the cell actually reacts to the indenter. The mass fraction of proteins in the cytoplasm can be up to 200 mg/ml, which is 20% of the total mass (Luby-Phelps, 1994). However, not all of these proteins belong to the cytoskeleton and not all of them are in the polymerized, filamentous form. But the large amount of proteins suggests that not only cytoplasm but also the cytoskeleton itself is deformed and maybe even pushed aside, especially in the flat structures like the filopodia that are substantially compressed during the force curves. An interesting project in the future might be disabling the molecules cross-linking the filaments of the cytoskeleton or disabling the molecules anchoring the cytoskeleton to the cell membrane and monitor the corresponding changes in the cell's viscoelastic properties.

In Fig. 12 we showed a topographic map and a map of the elastic properties of the same platelet obtained simultaneously by force mapping. The organization of activated platelets have been studied in depth with electron microscopy and a strong correlation of the topography and the underlying cytoskeleton has been found (Albrecht et al., 1989). Therefore we can discuss Fig. 12 in terms of the underlying organization of cellular features. We have denoted the visible parts of the cell with their standard nomenclature: pseudonucleus (P), inner filamentous zone (I), outer filamentous zone (O), and the cortex (C). The pseudonucleus consists mainly of granula, small vesicles filled with proteins and cytosol. This area is not surprisingly the softest part of the cell (1.5–4 kPa). The inner filamentous zone consists of the contractile apparatus of the platelet. There are zones of dense filament networks where myosin overlaps with actin polymers. The elasticity map shows regions that are approximately as soft as the pseudonucleus (4 kPa; thin, black arrows) but also shows areas that are slightly stiffer (10 kPa; thick, black arrow). The stiffer

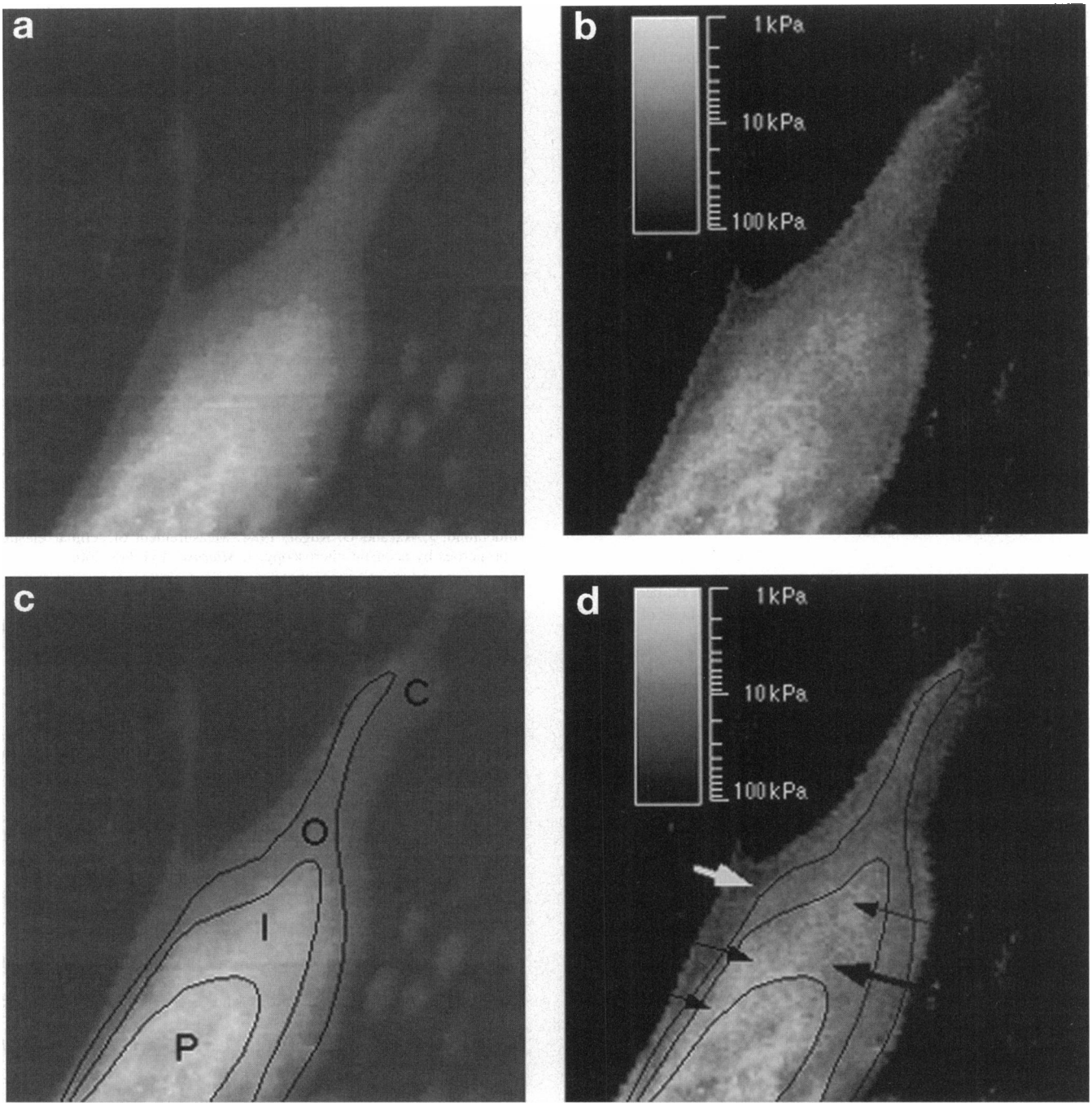

FIGURE 12 Topography and the elastic modulus calculated from all force curves taken over a human platelet and encoded in gray. The image size is 4.3 μm. The range of gray scales in *a* (the topography) is 2 μm. In *b*, the elastic modulus is encoded logarithmically so that black corresponds to 100 kPa and white corresponds to 1 kPa (see the gray scale bar in the image). In *c*, the different parts of the platelet with their usual nomenclature are outlined: the pseudonucleus (P), the inner web (I), the outer web (O), and the cortex (C). The pseudonucleus is softest (1.5 to 4 kPa), the inner web has a stiffness of ~4 kPa, the outer web ranges around 10–40 kPa. Some areas in the cortex (*white arrow*) are stiffest (50 kPa). There are some areas that deviate from the general patterns; see for instance the area the thick, black arrows are pointing to (10 kPa) or the area the thin, black arrows are pointing to (4 kPa).

parts may correspond to the zones with a dense network of myosin and filamentous actin right next to softer regions with a lower concentration of those polymers. The outer filamentous zone consists mainly of bundles of actin filaments and microtubules. It shows stiffnesses ranging from 10 to 40 kPa, which gradually turn into each other probably indicating a smooth change in distribution or concentration of the filaments rather than an abrupt border. The cortex consists of a dense homogeneous network of short actin filaments. It has in most areas similar stiffnesses except at a very flat region, which shows an elastic modulus up to 53 kPa (white arrow).

CONCLUSIONS

We have demonstrated that the AFM can be used to measure the elastic properties of cells in vivo. In this study we were able to determine the elastic modulus on human platelets with a lateral resolution of 100 nm. The elastic moduli ranged between 1 and 50 kPa, depending on position on the cell. This opens a new field of experiments in cell biology. As the cytoskeleton plays a major roll in such important fields as cell shape, cell motility, cell division, and cell adhesion, the additional knowledge about the stiffness of the cytoskeleton might lead to new insights in all of these fields. Platelets might be a very interesting system for future studies, as their cytoskeleton undergoes a huge reorganization during activation. This reorganization is related to the platelet's function and carefully controlled by the cell. Therefore the method described here might give new insights into the architecture of the cytoskeleton and its biological function, especially when combined with other techniques, such as interference light microscopy or fluorescent labeling, which can be performed simultaneously with the same cell.

We thank Cliff Farmer (Tri County Blood Bank, Santa Barbara, CA) for supplying us with fresh platelet concentrate in the early stages of this study. We also thank Digital Instruments for technical support.

This work was supported by a grant from the Materials Research Division of the National Science Foundation under NSF-DMR-9221781 (M. R. and P. K. H), the Deutsche Forschungsgemeinschaft (M. F.), and the Office of Naval Research (J. C.) and a fellowship of the Österreichisches Bundesministerium für Wissenschaft und Forschung (C. K.). This work was partially supported by the MRL Program of the National Science Foundation under award DMR-9123048 (C. K.).

REFERENCES

Adams, D. S. 1992. Mechanics of cell shape change: the cytomechanics of cellular response to chemical environment and mechanical loading. *J. Cell Biol.* 117:83–93.

Albrecht, R. M., S. L. Goodman, and S. R. Simmons. 1989. Distribution and movement of membrane-associated platelet glycoproteins: use of colloidal gold with correlative video-enhanced light microscopy, low-voltage high-resolution scanning electron microscopy, and high-voltage transmission electron microscopy. *Am. J. Anat.* 185:149–164.

Askin, A., and J. M. Dziedzic. 1989. Internal cell manipulation using infrared laser traps. *Proc. Natl. Acad. Sci. USA.* 86:7914–7918.

Baselt, D. R., and J. D. Baldeschwieler. 1994. Imaging spectroscopy with the atomic force microscope. *J. Appl. Phys.* 76:33–38.

Baselt, D. R., S. M. Clark, M. G. Youngquist, C. F. Spence, and J. D. Baldeschwieler. 1993. Digital signal processor control of scanned probe microscopes. *Rev. Sci. Instrum.* 64:1874–1882.

Bezanilla, M., B. Drake, E. Nudler, M. Kashlev, P. K. Hansma, and H. G. Hansma. 1994. Motion and enzymatic degradation of DNA in the atomic force microscope. *Biophys. J.* 67:1–6.

Binnig, G., C. F. Quate, and C. Gerber. 1986. Atomic force microscope. *Phys. Rev. Lett.* 56:930.

Burnham, N. A., and R. J. Colton. 1989. Measuring the nanomechanical properties and surface forces of materials using an atomic force microscope. *J. Vac. Sci. Technol.* A7(4):2906–2913.

Discher, D. E., N. Mohandas, and E. A. Evans. 1994. Molecular maps of red cell deformation: hidden elasticity and in situ connection. *Science.* 266:1032–1035.

Drake, B., C. B. Prater, A. L. Weisenhorn, S. A. C. Gould, T. R. Albrecht, C. F. Quate, D. S. Cannell, H. G. Hansma, and P. K. Hansma. 1989. Imaging crystals, polymers and biological processes in water with AFM. *Science.* 243:1586–1589.

Evans, E. 1989. Structure and deformation properties of red blood cells: concepts and quantitative methods. *Methods Enzymol.* 173:3–35.

Felder, S., and E. L. Elson. 1990. Mechanics of fibroblast locomotion: quantitative analysis of forces and motions at the leading lamellas of fibroblasts. *J. Cell Biol.* 111:2513–2526.

Florin, E.-L., V. T. Moy, and H. E. Gaub. 1994. Adhesion forces between individual ligand-receptor pairs. *Science,* 264:415–417.

Fritz, M., M. Radmacher, and H. E. Gaub. 1994a. Granula motion and membrane spreading during activation of human platelets imaged by atomic force microscopy. *Biophys. J.* 66:1328–1334.

Fritz, M., M. Radmacher, N. Petersen, and H. E. Gaub. 1994b. Visualization and identification of intracellular structures by force modulation microscopy and drug induced degradation. *J. Vac. Sci. Technol. B.* 12:1526–1529.

Hansma, H. G., and J. H. Hoh. 1994. Biomolecular imaging with the atomic force microscope. *Annu. Rev. Biophys. Chem.* 23:115–139.

Hartwig, J. H. 1992. Mechanisms of actin rearrangements mediating platelet activation. *J. Cell Biol.* 118:1421–1442.

Henderson, E. 1994. Imaging of living cells by atomic force microscopy. *Prog. Surface Sci.* 46:39–60.

Hertz, H. 1881. Über den Kontakt elastischer Körper. *J. Reine Angew. Mathematik.* 92:156.

Hildebrand, J. A., and D. Rugar. 1984. Measurement of cellular elastic properties by acoustic microscopy. *J. Microsc.* 134:245–260.

Hoh, J., and A. Engel. 1993. Friction effects in force curves. *Langmuir.* 9:3310–3312.

Hoh, J. H., and C.-A. Schoenenberger. 1994. Surface morphology and mechanical properties of MDCK monolayers by atomic force microscopy. *Biophys. J.* 107:1105–1114.

Janmey, P. 1991. Mechanical properties of cytoskeletal polymers. *Curr. Opin. Cell Biol.* 3:4–11.

Janmey, P. A., S. Hvidt, J. Käs, D. Lerche, A. Maggs, E. Sackmann, M. Schliwa, and T. P. Stossel. 1994. The mechanical properties of actin gels: elastic modulus and filament motion. *J. Biol. Chem.* 269: 32503–32513.

Karrasch, S., R. Hegerl, J. H. Hoh, W. Baumeister, and A. Engel. 1994. Atomic force microscopy produces faithful high-resolution images of protein surfaces in an aqueous environment. *Proc. Natl. Acad. Sci. USA.* 91:836–838.

Lee, G. U., L. A. Chris, and R. J. Colton. 1994. Direct measurement of the forces between complementary strands of DNA. *Science.* 266: 771–773.

Loftus, C. J., J. Choate, and R. M. Albrecht. 1984. Platelet activation and cytoskeletal reorganisation: high voltage electron microscopic examination of intact and Triton-extracted whole mounts. *J. Cell Biol.* 98: 2019–2025.

Luby-Phelps, K. 1994. Physical properties of cytoplasm. *Curr. Opin. Cell Biol.* 6:3–9.

Lüers, H., K. Hillman, J. Litniewski, and J. Bereiter-Hahn. 1991. Acoustic microscopy of cultured cells: distribution of forces and cytoskeletal elements. *Cell Biophys.* 18:279–293.

Peterson, N. O., W. B. McConnaughey, and E. L. Elson. 1982. Dependence of locally measured cellular deformibality on position on the cell, temperature and cytochalasin B. *Proc. Natl. Acad. Sci. USA.* 79: 5327–5331.

Putman, C. A. J., K. O. van der Werf, B. G. de Grooth, N. F. van Hulst, J. Greve, and P. K. Hansma. 1992. A new imaging mode in atomic force microscopy based on the error signal. *Proc. SPIE.* 1639:198–204.

Radmacher, M., M. Fritz, J. P. Cleveland, D. R. Walters, and P. K. Hansma. 1994b. Imaging adhesion forces and elasticity of lysozyme adsorbed on mica by atomic force microscopy. *Langmuir.* 10:3809–3814.

Radmacher, M., J. P. Cleveland, M. Fritz, H. G. Hansma, and P. K. Hansma. 1994a. Mapping interaction forces with the atomic force microscope. *Biophys. J.* 66:2159–2165.

Radmacher, M., M. Fritz, H. G. Hansma, and P. K. Hansma. 1994c. Direct observation of enzyme activity with the atomic force microscope. *Science.* 265:1577–1579.

Radmacher, M., M. Fritz, and P. K. Hansma. 1995. Imaging soft samples with the atomic force microscope: gelatin in water and propanol. *Biophys. J.* 69:264–270.

Radmacher, M., R. W. Tillman, and H. E. Gaub. 1993. Imaging viscoelasticity by force modulation with the atomic force microscope. *Biophys. J.* 64:735–742.

Radmacher, M., R. W. Tillmann, M. Fritz, and H. E. Gaub. 1992. From molecules to cells: imaging soft samples with the AFM. *Science.* 257: 1900–1905.

Sackmann, E. 1994. Intra- and extracellular macromolecular networks: physics and biological function. *Macromol. Chem. Phys.* 195:7–28.

Svoboda, K., C. F. Schmidt, D. Branton, and S. M. Block. 1992. Conformation and elasticity of the isolated red blood cell membrane skeleton. *Biophys. J.* 63:784–793.

Tao, N. J., N. M. Lindsay, and S. Lees. 1992. Measuring the microelastic properties of biological materials. *Biophys. J.* 63:1165–1169.

Weisenhorn, A. L., P. K. Hansma, T. R. Albrecht, and C. F. Quate. 1989. Forces in atomic force microscopy in air and water. *Appl. Phys. Lett.* 54:2651–2653.

Weisenhorn, A. L., P. Maivald, H.-J. Butt, and P. K. Hansma. 1992. Measuring adhesion, attraction, and repulsion between surfaces in liquids with an atomic force microscope. *Phys. Rev. B (Condensed Matter).* 45:11226–11232.

Yang, J., J. Mou, and Z. Shao. 1994. Molecular resolution atomic force microscopy of soluble proteins in solution. *Biochim. Biophys. Acta.* 1199:105–114.

Zahalak, G. I., W. B. McConnaughey. and E. L. Elson. 1990. Determination of cellular mechanical properties by cell poking, with an application to leukocytes. *J. Biomech. Eng.* 112:283–294.

Zeman, K., H. Engelhard, and E. Sackmann. 1990. Bending undulations and elasticity of the erythrocyte membrane: effects of cell shape and membrane organization. *Eur. Biophys. J.* 18:203–219.